J Membrane Biol (2014) 247:1005–1018
DOI 10.1007/s00232-014-9678-4

Amphipol-Trapped ExbB–ExbD Membrane Protein Complex from *Escherichia coli*: A Biochemical and Structural Case Study

Aleksandr Sverzhinsky · Shuo Qian · Lin Yang · Marc Allaire · Isabel Moraes · Dewang Ma · Jacqueline W. Chung · Manuela Zoonens · Jean-Luc Popot · James W. Coulton

Received: 29 January 2014 / Accepted: 9 May 2014 / Published online: 27 May 2014

Abstract Nutrient import across Gram-negative bacteria's outer membrane is powered by the proton-motive force, delivered by the cytoplasmic membrane protein complex ExbB–ExbD–TonB. Having purified the $ExbB_4$–$ExbD_2$ complex in the detergent dodecyl maltoside, we substituted amphipol A8-35 for detergent, forming a water-soluble membrane protein/amphipol complex. Properties of the $ExbB_4$–$ExbD_2$ complex in detergent or in amphipols were compared by gel electrophoresis, size exclusion chromatography, asymmetric flow field-flow fractionation, thermal stability assays, and electron microscopy. Bound detergent and fluorescently labeled amphipol were assayed quantitatively by 1D NMR and analytical ultracentrifugation, respectively. The structural arrangement of $ExbB_4$–$ExbD_2$ was examined by EM, small-angle X-ray scattering, and small-angle neutron scattering using a deuterated amphipol. The amphipol-trapped $ExbB_4$–$ExbD_2$ complex is slightly larger than its detergent-solubilized counterpart. We also investigated a different oligomeric form of the two proteins, $ExbB_6$–$ExbD_4$, and propose a structural arrangement of its transmembrane α-helical domains.

Keywords Membrane protein complex · Amphipol · Detergent · EM · SAXS/SANS

Introduction

Gram-negative bacteria contain a cell envelope consisting of an outer membrane (OM) and a cytoplasmic membrane (CM), that are separated by the periplasm. The OM, acting as a physical barrier between the external milieu and the

Electronic supplementary material The online version of this article (doi:10.1007/s00232-014-9678-4) contains supplementary material, which is available to authorized users.

A. Sverzhinsky · J. W. Chung · J. W. Coulton
Department of Microbiology and Immunology, McGill University, Montreal H3A 2B4, QC, Canada

S. Qian
Center for Structural Molecular Biology and Biology and Soft Matter Division, Oak Ridge National Laboratory, Oak Ridge, TN 37831, USA

L. Yang · M. Allaire
Photon Sciences Directorate, Brookhaven National Laboratory, Upton, NY 11973, USA

I. Moraes
Membrane Protein Laboratory, Diamond Light Source, Didcot OX11 0DE, UK

I. Moraes
Research Complex at Harwell Appleton Laboratory, Harwell Science and Innovation Campus, Didcot OX11 0DE, UK

I. Moraes
Department of Life Sciences, Imperial College London, London SW7 2AZ, UK

D. Ma
Faculté de Pharmacie and Département de Chimie, Université de Montréal, Montreal H3C 3J7, QC, Canada

M. Zoonens · J.-L. Popot
Laboratoire de Biologie Physico-Chimique des Protéines Membranaires, UMR 7099, Paris, France

M. Zoonens · J.-L. Popot
CNRS/Université Paris 7, Institut de Biologie Physico-Chimique (FRC 550), Paris, France

J. W. Coulton (✉)
Microbiome and Disease Tolerance Centre, 3775 University Street, Montreal, QC H3A 2B4, Canada
e-mail: james.coulton@mcgill.ca

cellular interior, is also the site of nutrient import. Small nutrients (<600 Da) diffuse through porins, whereas larger nutrients such as vitamin B_{12} and iron-bound siderophores must be actively imported by a special class of membrane proteins (MPs): OM receptors (Nikaido 2003). The import of these essential nutrients contributes to the establishment of infection, making this process an attractive target for therapeutic agents. Whereas different OM receptors facilitate transport of their respective nutrients, the necessary energy comes from a common CM-embedded MP complex: ExbB–ExbD–TonB (Braun et al. 1996). ExbB (26.3 kDa) is considered to be the complex's scaffolding protein (Pramanik et al. 2010). It is predicted to feature three transmembrane (TM) α-helices, with most of its hydrophilic amino acids located in the cytoplasm (Baker and Postle 2013; Kampfenkel and Braun 1993). ExbB stabilizes TonB (26.0 kDa) and ExbD (15.5 kDa) via their TM α-helical domains (Baker and Postle 2013). TonB and ExbD are predicted to each have a short cytoplasmic N-terminus, a single TM α-helix, and a C-terminus localized in the periplasm (Chu et al. 2007; Kampfenkel and Braun 1992). TonB spans the periplasm and links OM receptors to the energy of the proton-motive force of the CM (Krewulak and Vogel 2011; Pawelek et al. 2006). However, ExbD is the only protein in the complex able to respond to the proton-motive force (Ollis et al. 2012). ExbB and ExbD have previously been shown to form heterodimers (Jana et al. 2011) and have been co-purified using affinity chromatography (Pramanik et al. 2011). The latter study found ExbB to be mostly hexameric ($ExbB_6$) by laser-induced liquid bead ion desorption mass spectrometry (LILBID-MS), whereas the former study found it to be tetrameric ($ExbB_4$) by in vivo cross-linking.

We previously co-purified ExbB and ExbD by immobilized metal ion affinity chromatography (IMAC) via an engineered hexa-histidine tag (His_6 tag) at ExbD's C-terminus (16.7 kDa; Sverzhinsky et al. 2014). Whereas the two proteins solubilized in *n*-dodecyl-*β*-D-maltopyranoside (DDM) were electrophoretically pure, they formed multiple complexes of varying stoichiometries. Screening of various detergents concluded that DDM was the optimal detergent in terms of monodispersity and long-term stability. The principal ExbB–ExbD complex had a stoichiometry 4:2. The calculated 138.6 kDa of protein (based on theoretical molecular masses) would comprise 14 TM α-helices, forming a protein/detergent complex of ~240 kDa. After purifying a single monodisperse fraction by size exclusion chromatography (SEC) and observing it by negative stain electron microscopy (EM), we reconstructed the $ExbB_4$–$ExbD_2$ complex in three structural states, the maps being resolved to ~21–27 Å. The ExbD periplasmic domain was unambiguously identified on one side of the TM region, thereby localizing the bulky cytoplasmic domains of ExbB on the opposite side. Whereas we were able to interpret the different structural states in terms of domain flexibility, we wished to gain structural information on the TM domains.

Amphipols (APols) are short amphipathic polymers designed to substitute for detergents at the TM surface of MPs, thereby keeping them water-soluble and stabilizing them (Tribet et al. 1996; Popot et al. 2011; Zoonens and Popot 2014). The most widely used and best-characterized APol, called A8-35, is obtained by grafting randomly a short polyacrylate main chain with ~25 % octylamine and ~40 % isopropylamine side chains, leaving ~35 % of the carboxylates free (Tribet et al. 1996; Gohon et al. 2004, 2006). A8-35 molecules are polydisperse, with an average mass of ~4.3 kDa (Giusti et al. 2014). In aqueous solutions, above a concentration of ~0.002 g/L (Giusti et al. 2012), they self-organize (Perlmutter et al. 2014) into globular, micelle-like particles with an average mass of ~40 kDa (Gohon et al. 2006). Trapping a MP in APols is usually achieved by adding the APol to the detergent-solubilized MP and removing the detergent, e.g., by adsorption onto polystyrene beads (for detailed protocols, see Zoonens et al. 2014). To a large extent, MP/APol complexes can be handled in surfactant-free solutions as though they were soluble proteins, and their structure studied by such approaches as EM, small-angle X-ray and neutron scattering (SAXS and SANS, respectively), NMR, and analytical ultracentrifugation (AUC) (reviewed in Popot et al. 2011; Zoonens and Popot 2014). However, the presence of a small excess of APol over that bound to the protein is essential to preserving the monodispersity of the complexes (Zoonens et al. 2007; Gohon et al. 2008; Arunmanee et al. 2014; Charvolin et al. 2014; for a discussion, see Zoonens and Popot 2014). Here, we compare structural information gathered on APol-trapped and DDM-solubilized ExbB–ExbD complexes.

Materials and Methods

Cloning and Expression

The *E. coli exbBD* operon was PCR amplified and cloned into plasmid pQE60 containing an ampicillin-resistance marker (QIAGEN) and appending a His_6 tag to the C-terminus of ExbD. This plasmid was introduced into *E. coli* strain M15, harboring the pREP4 plasmid containing a kanamycin-resistance marker (QIAGEN) and encoding a Lac repressor for strict expression of recombinant proteins. *E. coli* M15 cells containing both plasmids were grown in 1 L of Terrific Broth supplemented with 50 μg/mL ampicillin, 30 μg/mL kanamycin, 10 % (v/v) glycerol, and potassium phosphate pH 8.0. Having reached an A_{600} of

1.0–1.2 (shaking at 37 °C), 0.5 mM isopropyl-β-D-1-thiogalactoside (Bio Vectra) was added to induce protein expression for 4 h at 24 °C. Cells were sedimented and stored at −20 °C until use.

Purification, Protein and Detergent Analysis

Thawed bacterial cell pellets were suspended in 25 mL lysis buffer containing 50 mM Tris pH 8.0, 200 mM NaCl, 5 mM $MgCl_2$, 100 µg/mL DNAse I, 100 µg/mL RNAse A, 10 µg/mL lysozyme, and one tablet of mini-complete protease inhibitor cocktail (Roche). Cells were lysed by two passages through an Emulsiflex homogenizer (Avestin) at 17,500 kPa. Following removal of debris by low-speed centrifugation, the supernatant was ultracentrifuged at 250,000×*g* for 1 h at 4 °C; membranes were collected and then solubilized for 1.5 h at 4 °C in 25 mL of solubilization buffer containing 50 mM Tris pH 7.5, 200 mM NaCl and 1 % (w/v) DDM (Glycon) with mini-complete protease inhibitor cocktail. The solubilized material was clarified (34,500×*g* centrifugation for 45 min) and applied onto 5 or 25-mL Profinity (Bio-Rad) IMAC column equilibrated with 50 mM Tris pH 7.5, 200 mM NaCl, and 0.02 % (w/v) DDM. After a 35 mM imidazole washing step, specifically-bound material was eluted in 25 mM Tris pH 7.5, 100 mM NaCl, 200 mM imidazole, and 0.02 % (w/v) DDM.

Protein concentrators with 150 kDa molecular weight cut-off (MWCO; Thermo Scientific) were used to concentrate protein samples (2,000×*g* centrifugations in a Sorvall H-6000 hanging bucket rotor). Further purification of concentrated material was done by preparative SEC using a 24-mL (10 × 300 mm) Superose 6 GL (GE Healthcare) column or a 120-mL (16 × 600 mm) Superdex 200 pg (GE Healthcare) column at 0.5 and 1.0 mL/min flow-rates, respectively.

Protein was measured using the NanoDrop 1000 (Thermo Scientific) and appropriate ExbB–ExbD complex extinction coefficients (Pace et al. 1995). Absorbance readings greater than 1.0 were corrected where necessary due to deviation from linearity of the Beer–Lambert law (Aitken and Learmonth 2002).

To evaluate protein content, samples were analyzed by SDS-PAGE separation followed by silver staining or by Coomassie Blue G-250 staining. For the latter, relative molar abundance was determined using the ImageJ software suite (Schneider 2012). Migration distances were compared to PageRuler protein standards (Thermo Scientific).

Detergent quantitation was performed as previously described (Maslennikov et al. 2007). Samples were fractionated on the Superose 6 SEC column in 25 mM glycine pH 9, 150 mM NaCl, 0.02 % (w/v) DDM. Individual fractions were diluted by 20 % (final volume 650 µL) with an internal standard, 2,2-dimethyl-2-silapentane-5-sulfonic acid (DSS) solution in D_2O (Sigma). 1D NMR spectra were recorded at the Quebec and Eastern Canada NMR Facility on a Varian INOVA 500 MHz spectrometer. Comparison of integrated detergent peaks to integrated DSS standard peaks allowed calculation of detergent concentration in each fraction. Specifically, a single DSS peak resulting from nine identical protons at 0 ppm was compared to a single DDM peak resulting from the molecule's three protons on the terminal carbon at 0.84 ppm.

Amphipol-Trapping

IMAC-purified protein samples in DDM were supplemented with APol A8-35 (Anatrace) at a 1:5.6 protein/APol mass ratio, rocked at 4 °C for 20 min, and DDM removed by rocking incubation with a 64 × excess (w/w) BioBeads SM-2 (Bio-Rad) over DDM for 2 h at 4 °C (Holloway 1973). Subsequent buffers contained 25 mM Tris pH 7.5, 150 mM NaCl, no surfactant. Protein/APol complexes were recovered in the supernatant following ultracentrifugation at 100,000×*g* for 20 min.

For measurement of protein-bound APol, IMAC-purified protein samples were trapped with 7-nitro-1,2,3-benzoxadiazole-4-yle (NBD-labeled) A8-35 (hereafter FAPol, for 'fluorescent APol'; synthesized by F. Giusti, UMR 7099; see Zoonens et al. 2007), diluted with commercial (hydrogenated) APol in a 1:5 mass ratio. The specific FAPol preparation contained ∼1 molecule of NBD per 48 kDa of polymer (Zoonens et al. 2007). Its optical densities in 20 mM Tris pH 8.5 and 100 mM NaCl at 280 and 490 nm were 0.0339 and 0.1008 L/(g cm), respectively, before dilution with APol.

Some of the samples used for SANS/SAXS measurements were trapped in A8-35 with deuterated side chains (DAPol; synthesized by F. Giusti). The contrast-matching point of pure DAPol is ∼85 % D_2O (Gohon et al. 2004, 2006).

Analysis of Complex Size

Native Gel Electrophoresis

Native protein samples were analyzed by blue-native PAGE (BN-PAGE) using 4–20 % acrylamide gradient gels infused with 0.05 % (w/v) DDM. Samples, along with protein standards (NativeMark, Life Technologies), were run on ice at 100 V with cathode buffer (25 mM Tris and 192 mM glycine pH 8.8) containing 0.02 % (w/v) Coomassie Blue G-250. After 45 min, the blue cathode buffer was replaced with clear cathode buffer and electrophoresis was continued for 3 h at 200 V.

Analytical Size Exclusion Chromatography

Stokes radii (R_{st}) of ExbB–ExbD complexes were compared to protein standards of known R_{st} (Bio-Rad) by analytical SEC using the Superose 6 column or a 24-mL (10 × 300 mm) Superdex 200 GL (GE Healthcare) column at 0.5 mL/min flow-rates.

Asymmetric Flow Field-Flow Fractionation

Independent measures of R_{st} by different biophysical criteria were achieved by asymmetric flow field-flow fractionation (AF4). APol-trapped samples in buffer containing 25 mM Tris pH 7.5, 100 mM NaCl, and 50 mM imidazole at 1.6 mg/mL were injected onto an AF2000 (Postnova Analytics) linked to a SPD-20A UV–Vis detector (Shimadzu Corporation), multi-angle laser light scattering (MALLS) and quasi-elastic light scattering using a DAWN HELEOS 8 (Wyatt Technology) at 658 nm. The separation channel had a thickness of 350 µm, a length of 280 mm and contained regenerated cellulose membrane with a MWCO of 5 kDa. Elution peaks were analyzed with the ASTRA software package (version 5.3.4.20; Wyatt Technology). Injection of the sample (20 µL) used a flow rate of 0.2 mL/min. Detector flow rate was kept constant at 0.5 mL/min. The total focusing period was 5 min with a focus flow at 2.0 mL/min. The separation step began with a cross flow of 1 mL/min for 15 min, then a linear decrease to zero cross flow within 10 min, followed by 5 min of zero cross flow. Experiments were carried out at room temperature (23 °C).

Size Exclusion Chromatography with Multi-angle Laser Light Scattering

Detergent-solubilized IMAC-purified samples were analyzed by MALLS coupled to the 120-mL Superdex 200 column (SEC–MALLS) using light scattering detectors at 656 nm (miniDAWN TREOS; Wyatt Technology) under the control of an Alliance HPLC (Waters Corporation). Inter-detector delay was corrected using aldolase (GE Healthcare) in the ASTRA software package suite (version 5.3.4.18; Wyatt Technology). Total complex size was measured using theoretical *dn/dc* values derived from mixtures of DDM (0.143 mL/g) (Roy et al. 2013; Salvay and Ebel 2006) and protein (0.187 mL/g for most ExbB–ExbD stoichiometries based on SEDFIT (Schuck 2000) and considered the accepted value for MPs (Hayashi et al. 1989)).

Thermal Stability Assay

The thermal stability of IMAC-purified samples was determined at the Membrane Protein Laboratory, Diamond Light Source as previously reported (Alexandrov et al. 2008). Thiol-specific fluorochrome *N*-[4-(7-diethylamino-4-methyl-3-coumarinyl)phenyl]maleimide (CPM; Sigma) was added to protein samples at a final concentration of 28 µg/mL. Fluorescence was measured in a 7500 Fast Real-Time PCR System (AB Applied Biosystems), while heating with a ramp rate of 1 °C/min up to 95 °C.

Electron Microscopy

SEC-purified protein was used to prepare grids for EM at the Facility for Electron Microscopy Research, McGill University. DDM-solubilized samples from the 120-mL Superdex 200 column or APol-trapped samples from the 24-mL Superose 6 column were adsorbed for 1 min on negatively glow-discharged carbon-coated EM copper grids. After blotting excess liquid, 5 µL of freshly prepared 1.5 % (w/v) uranyl formate (pH 5) was added to the DDM-solubilized sample for 1.5 min and 5 µL of 2 % (w/v) uranyl acetate (pH 4) was added to the APol-trapped sample for 1 min, then removed. Digital micrographs were recorded on a FEI Tecnai G2 F20 having a Gatan Ultrascan 4 × 4 k Digital CCD Camera System at a nominal magnification of 68,000× corresponding to a pixel size 2.2 Å at specimen level. Images were recorded at defocus between 1.5 and 3.5 µm.

Particles were selected using the software suite Signature (Chen and Grigorieff 2007), boxed (128 × 128-pixel images) and normalized with Xmipp (Scheres et al. 2008). Two-dimensional (2D) class averages were created using the program Iterative Stable Alignment and Clustering (Yang et al. 2012).

Analytical Ultracentrifugation

SEC-purified samples were analyzed on a Beckman Coulter XL-I analytical ultracentrifuge with an An-60 Ti rotor, using 12-mm path length double channel centerpieces and the UV–VIS optics detection system. The centerpieces were filled with 390 µL of FAPol-trapped samples and 400 µL of reference buffer (25 mM Tris pH 7.5, 150 mM NaCl). Sedimentation velocity (SV) was measured overnight at 40,000 rpm at 20 °C, recording at dual wavelengths: 280 and 490 nm. $c(s)$ analysis used scans 6–324 (490 nm) and 7–325 (280 nm) in SEDFIT. Allowing parameters to float resulted in a frictional ratio of 1.4 (280 nm data) and rmsd of 0.0041. Similar parameters were applied to the 490 nm data, resulting in rmsd of 0.0053 (with a resolution = 200).

Small-Angle X-ray and Neutron Scattering

SAXS data were collected at beamline X9 of the National Synchrotron Light Source, using the standard solution

scattering setup previously described (Allaire and Yang 2011). The samples were measured at 10 °C and the X-ray energy was 13 keV. The 1D scattering profiles were obtained using the pyXS software that performs all necessary data corrections and buffer scattering subtraction (Yang 2013). Measurements were recorded on supplemented protein/APol complexes, free APols (9.1 mg/mL), and free DAPols (9.1 mg/mL) using appropriate blank buffers.

SANS data were collected at the Bio-SANS beam line of Oak Ridge National Laboratory (Lynn et al. 2006). The protein solution samples and corresponding buffer backgrounds were measured in 1-mm path length quartz cells at ~10 °C. The wavelength of the neutron was set to $\lambda = 6$ Å with the wavelength spread $\Delta\lambda/\lambda = 15$ %. Two detector-to-sample distances, 1.1 and 6.8 m, were used to produce a q range from ~0.008 to 0.4 Å^{-1}, falling into the relevant length scale for protein studies. The scattered data were collected by a 2-dimensional position-sensitive detector of 192 by 256 pixels developed by Oak Ridge National Laboratory. The 1D profile $I(q)$ versus q, where $q = 4\pi \sin(\theta)/\lambda$ and 2θ is the scattering angle from the incident beam, was obtained by azimuthally averaging from the 2D data, corrected for detector's electronic noise, ambient background radiation, detector pixel sensitivity, geometry distortion, and buffer background scattering. Data reduction was done using Mantid software (mantidproject.org). A constant background representing the difference in incoherent scattering resulting from the differences in hydrogen content of the samples and backgrounds was further subtracted from the 1D profile. The ExbB–ExbD sample was dialyzed against a buffer containing 85 % D_2O at 4 °C overnight before SANS measurements. The 85 % D_2O ratio was selected to contrast match with the scattering length density of DAPol (Gohon et al. 2004). The molecular weight of the protein complex, therefore, can be determined from the shape-independent function of the total scattering $I(0)$:

$$M.W = \frac{I(0) * N_A}{C((\rho_{protein} - \rho_{buffer}) * V_s)^2} \quad (1)$$

where N_A is Avogadro's number; C is the concentration of the protein in solution. The neutron scattering length densities of the protein and buffer are $\rho_{protein}$ and ρ_{buffer}, respectively. V_s is the specific volume of the scattering particle, which in this work has been estimated from the protein specific volume of 0.74 cm^3/g (Harpaz et al. 1994). The radius of gyration (R_g) was determined using Guinier approximation (Heller 2010):

$$I(q) = I(0)e^{-q^2R_g^2/3} \quad (2)$$

where $I(0)$ is the forward scattering. The Guinier plot, a linear fit of $\ln(I(q))$ versus q^2 with the restriction of $q^*R_g < 1.3$, is able to provide $I(0)$ and R_g. Low-q data were discarded due to the concern of minor contamination by aggregates. The distance distribution function $P(r)$ and maximum dimension D_{max} were obtained using the indirect Fourier transform method implemented in the program GNOM (Svergun 1992).

Results and Discussion

Solution Properties of ExbB–ExbD in DDM versus ExbB–ExbD in APols

Following solubilization in 1 % DDM, protein/detergent complexes were purified by IMAC and analyzed by SDS-PAGE separation with silver staining (Fig. 1a; lane 4). The

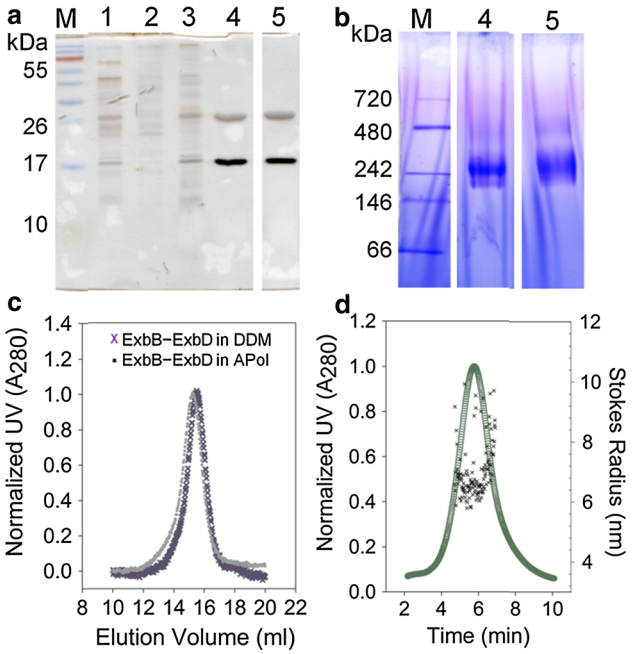

Fig. 1 ExbB–ExbD complexes are biochemically similar in DDM and in APols. **a** Protein separation by SDS-PAGE followed by silver staining identifies bands in total cell lysate (*lane 1*), the soluble fraction (*lane 2*) and the insoluble membrane fraction (*lane 3*). The two prominent proteins, ExbB and ExbD (migrating to ~26 and 17 kDa, respectively) are the sole proteins present after IMAC purification in DDM (*lane 4*) and following APol-trapping (*lane 5*). **b** BN-PAGE separation of the same samples as in (**a**) shows a prominent complex migrating close to the 242-kDa marker, with a faint complex migrating slightly further than the 480-kDa marker. The APol-trapped complex (*lane 5*) appears more polydispersed and has a slightly retarded migration as compared to the DDM-solubilized one (*lane 4*). M indicates molecular mass markers. **c** By analytical SEC using the 24-mL Superose 6 SEC column the DDM-solubilized and APol-trapped complexes elute similarly. A minor leading shoulder is discernible at ~13 mL. **d** An independent measurement of Stokes radius by AF4-MALLS confirms the apparent sizes of protein/APol complexes seen in (**c**). Later-eluting material has a larger R_S

sole proteins, migrating with M_r of ~26 and ~17 kDa, were submitted to mass spectrometry and identified as ExbB and ExbD, respectively (data not shown). Considering that only ExbD is His_6-tagged, the co-elution of ExbB indicates that the two proteins form a complex. Once separated by BN-PAGE, the principal protein/detergent complex migrates close to the 242 kDa protein marker (Fig. 1b; lane 4), consistent with the mass expected for an $ExbB_4$–$ExbD_2$ complex (138.6 kDa, based on theoretical molecular masses) with detergent bound to it.

Addition of various amounts of A8-35, followed by detergent removal and centrifugation, indicated that an APol/protein mass ratio of 5.6:1 ensured complete retention in solution of the detergent-free ExbB–ExbD complexes. With regards to detergent removal, a 64:1 mass ratio of BioBeads over DDM resulted in complete precipitation of the complexes in the absence of APol.

It has been observed previously that, in detergent solution, ExbB and ExbD co-purify primarily in the 4:2 stoichiometry, but they may form oligomers with other stoichiometries. Trapping the IMAC-purified sample in A8-35 resulted in the same oligomers, without any change in their relative distribution. DDM-solubilized and APol-trapped post-IMAC complexes had identical profiles upon denaturing SDS-PAGE (Fig. 1a; lanes 4 and 5). The principal complex migrated to a comparable distance by BN-PAGE separation (Fig. 1b; lane 5). However, the band of APol-trapped complex is slightly broader, suggesting greater size and/or charge polydispersity. It also migrated to a slightly higher apparent MW with respect to DDM-solubilized protein. This difference in size of the complex was reflected by analytical SEC (Fig. 1c). Compared to the apparent R_S of 6.2 nm for DDM-solubilized complex, the APol-trapped complex has a R_S of 6.5 nm. Because interactions of MP/A8-35 complexes with the resin of SEC columns have been shown to affect elution volumes (Zoonens et al. 2007), it was deemed interesting to examine the behavior of the complexes by AF4. This emerging technique, usually applied to polymers in aqueous solution (Giddings 1993; Wagner et al. 2014), separates particles not by interaction with a stationary phase, but solely between the particles and an external physical field, in this case buffer cross flow (Cölfen and Antonietti 2000). The APol-trapped complex radius was confirmed by AF4 coupled to MALLS, resulting in an average of 7.0 ± 0.9 nm and a median of 6.7 nm (Fig. 1d). Late-eluting particles at ~7 min, due to stronger retention by the cross flow, had relatively larger Stokes radii (discussed below).

Stabilization of ExbB–ExbD Complexes by Transfer to A8-35

MPs as a rule gain stability when trapped in APols (Popot et al. 2011; Zoonens and Popot 2014). The CPM assay was used to compare the thermal stability of DDM-solubilized *versus* A8-35-trapped ExbB–ExbD complexes. ExbD has no cysteine residues, but ExbB contains a single cysteine residue in its first TM α-helix (Baker and Postle 2013) that has been exploited as a sensor for the status of overall unfolding (Alexandrov et al. 2008). DDM-solubilized ExbB–ExbD has a melting temperature of 47 °C. A8-35-trapped ExbB–ExbD is significantly more thermally stable, with a T_m of 63 °C (data not shown). This 16-degree increase is larger than that (~11 °C) observed with a G protein-coupled receptor, the BLT1 receptor of leukotriene B_4. A8-35-trapped BLT1 is completely stable over a three-week period at 4 °C, whereas, over the same period, detergent-solubilized BLT1 loses about 50 % of its ligand-binding activity (Dahmane et al. 2009). On this basis, A8-35-trapped ExbB–ExbD can be expected to have a much longer shelf life than its DDM-solubilized form.

Electron Microscopy Investigation of the Complexes

The APol-trapped and DDM-solubilized forms of $ExbB_4$–$ExbD_2$ were compared by EM. In an earlier study, the DDM-solubilized complex obtained after fractionation on a 120-mL Superdex 200 SEC column was studied after staining with uranyl formate (Sverzhinsky et al. 2014). In the present work, APol-trapped ExbB–ExbD was purified on a 24-mL Superose 6 SEC column and the pooled peak fractions stained with uranyl acetate (Fig. 2a). The APol-trapped particles are virtually indistinguishable from the DDM-solubilized particles (Fig. 2a, b; white circles, enlarged in the insets), except that the Superose 6 SEC purification did not fully remove the larger oligomers (Fig. 2a; yellow circle). 2D image analysis revealed that, despite the use of a different metal stain (Ohi et al. 2004), the APol-trapped $ExbB_4$–$ExbD_2$ displayed features common to the DDM-solubilized particles (Fig. 2c). A thick (~4 × 10 nm) central density, previously identified as the TM region (red brackets), is expected to contain 14 TM α-helices (12 from ExbB and 2 from ExbD), plus the bound surfactant. Previous labeling experiments using Ni–NTA-Nanogold differentiated between the cytoplasmic and periplasmic sides of the TM region, identifying the periplasmic domain (comprising almost exclusively the ExbD C-terminus) as the sole extension from the TM region seen in Fig. 2c (upper panel). This density is not consistently observable in side views (*cf.* Fig. 2c, central panel), presumably because the C-termini are usually not dimerized, in which case their mass is insufficient for detection by negative stain EM. The cytoplasmic side of the TM region contains the cytoplasmic loops and C-termini of 4 ExbB molecules, interacting as a dimer of dimers, with some flexibility.

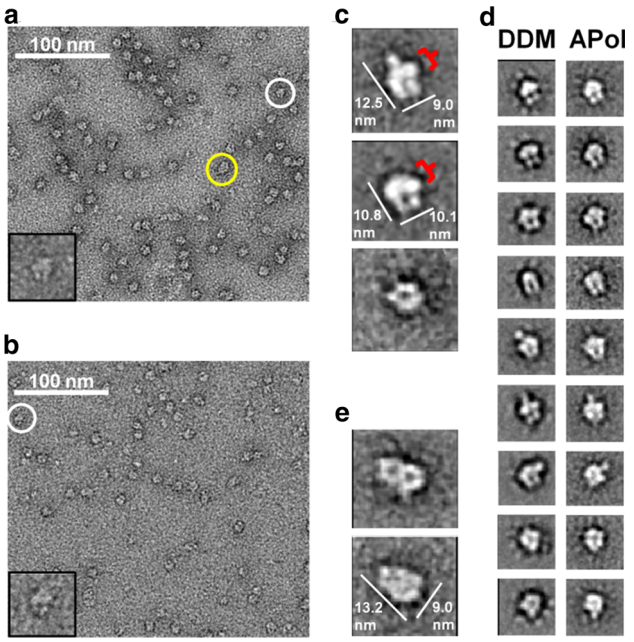

Fig. 2 Electron microscopy of APol-trapped ExbB–ExbD matches structural features of the DDM-solubilized complex. APol-trapped (**a**) and DDM-solubilized (**b**) electron micrographs display similar particles (*white circles*, enlarged in the *insets*). APol-trapped samples, which were purified on a 24-mL Superose 6 SEC column, also show a minority of larger oligomers (*yellow circle*). **c** Two-dimensional class averages of the APol-trapped $ExbB_4$–$ExbD_2$ complex identify the TM region (*red brackets*), the structurally dynamic periplasmic domain (isolated extension in the *upper panel*), and the cytoplasmic domains (*upper* and *central panels*). The *lower panel* is a bottom view showing the ring-like arrangement of the cytoplasmic domains. **d** APol-trapped $ExbB_4$–$ExbD_2$ shows all characteristic conformations of the DDM-solubilized complex. **e** The larger oligomer has a longer dimension than the complex in (**c**) as seen from the bottom (*upper panel*) and oblique (*lower panel*) orientations

Class averages of APol-trapped $ExbB_4$–$ExbD_2$ revealed similar dimensions as the DDM-solubilized complex: 9.0–10.1 nm diameter across (presumably the width in the membrane plane) and 10.8–12.5 nm long. Considering that we found class averages of APol-trapped $ExbB_4$–$ExbD_2$ in all of the characteristic DDM-solubilized conformations (Fig. 2d), we extrapolated our interpretation of coordinated rearrangements to the APol-trapped complex. Briefly, we hypothesize that the cytoplasmic domains assemble into a tetramer, forming a ring at the distal end (Fig. 2c lower panel) when ExbD's periplasmic domains are not dimerized, and therefore, not observable by negative stain EM. Upon dimerization of the periplasmic domains, the cytoplasmic domains rearrange into two thicker densities (each comprising two ExbB cytoplasmic domains) that form a compact arrangement at the distal end (Sverzhinsky et al. 2014). With the observation that the dimerized ExbD periplasmic domain is found in multiple positions with respect to the TM region, we conclude that the ExbB–ExbD complex possesses intrinsic conformational flexibility, which is most likely necessary for function (Ollis et al. 2012). APols appear to permit this flexibility.

Nature and Organization of the Larger ExbB–ExbD Oligomer

Two-dimensional classification of EM particles also shed light on the larger oligomer of ExbB–ExbD that purifies along with the $ExbB_4$–$ExbD_2$ complex. Figure 2e shows a bottom view (upper panel) and an oblique view (lower panel) of the APol-trapped larger oligomer that is longer (13.2 nm) than the 4:2 complex. This larger oligomer was seen by BN-PAGE (Fig. 1b; faint upper band), by analytical SEC (Fig. 1c; shoulder at ~14 mL) and by AF4 (Fig. 1d; increased particle sizes at ~7 min). To quantitate the size of this protein/detergent complex, we performed a SEC–MALLS experiment on the DDM-solubilized IMAC-purified ExbB–ExbD complex using the 120-mL Superdex 200 SEC column (Fig. 3a). With composite *dn*/*dc* values based on an approximate detergent contribution of 37 % (see below), the larger oligomer was found to have a molecular mass of 407.3 ± 5.7 kDa. This estimate is supported by BN-PAGE of the post-IMAC protein (Fig. 3b; lane 1), as well as pooled SEC fractions of this peak (Fig. 3b; lane 2). The soluble marker proteins form an excellent regression curve ($R^2 = 0.9999$), leading to an estimate of 382 kDa for the larger oligomer, potentially (Wasiak et al. 2002) a slight underestimate. Whereas this SEC column led to a greater separation of different oligomers of ExbB–ExbD than the 24-mL Superose 6 column, overlapping elution peaks representing these oligomers could not be resolved for quantitative Coomassie staining. However, the average of two fractions containing the elution peak of the larger oligomer (Fig. 3a; arrowheads) revealed an ExbB:ExbD molar ratio of ~3:2 (Fig. 3c). Considering the ~380–405 kDa protein/detergent complex and taking into account probable detergent contribution, this ratio corresponds to a 6:4 stoichiometry ($ExbB_6$–$ExbD_4$), calculated to comprise 224.7 kDa of protein.

Hexameric ExbB has previously been identified using LILBID-MS (Pramanik et al. 2011), among other stoichiometries, when ExbB-His_6 and ExbD-StrepII (both C-terminal) were co-purified. The elution of the larger oligomer just before the main peak on the same SEC column (24-mL Superose 6; Fig. 1c) is virtually identical in the two studies. However, Pramanik et al. did not observe any oligomeric ExbD, despite in vivo cross-linking evidence (Ollis and Postle 2011). The $ExbB_6$–$ExbD_4$ stoichiometry may facilitate sequestration of partially formed subunits for rapid assembly upon substrate binding to OM receptors, or it may represent another active stoichiometry in vivo. If ExbB and ExbD function akin to their flagellar homologues

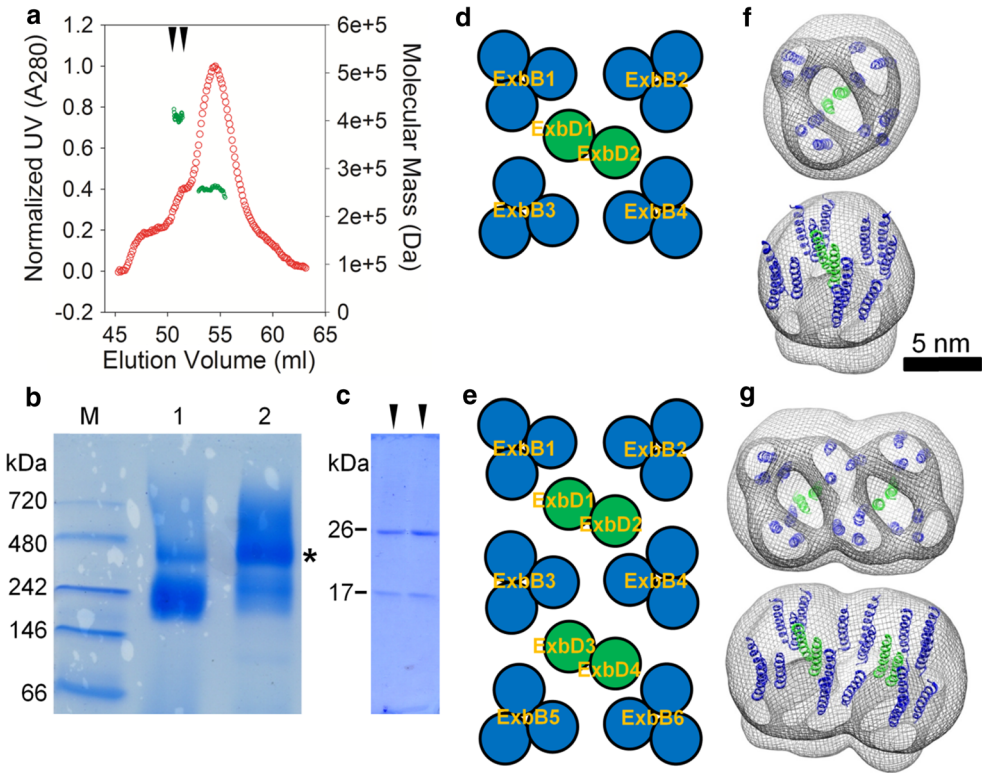

Fig. 3 A minority of ExbB–ExbD complexes form a larger oligomer of 6:4 stoichiometry. DDM-solubilized ExbB–ExbD predominantly forms a 4:2 complex (~240 kDa) but also forms a larger oligomer (~380–405 kDa) as seen by SEC–MALLS (**a**) and BN-PAGE (**b**). When analyzed by BN-PAGE, this complex migrates to ~380 kDa (*asterisk*) in the pre-SEC sample (*lane 1*) and in pooled SEC fractions (*lane 2*). M shows molecular mass markers. **c** A molar ratio of 3 ExbB: 2 ExbD was quantitated from Coomassie staining of isolated fractions (*arrowheads* in (**a**)) separated by SDS-PAGE, indicative of a $ExbB_6$–$ExbD_4$ complex. Based on EM observations and models proposed by others, a hypothetical arrangement of TM α-helices is shown for the $ExbB_4$–$ExbD_2$ (**d**) and $ExbB_6$–$ExbD_4$ (**e**) complexes. TM α-helices were then modeled into our EM map of (**f**) $ExbB_4$–$ExbD_2$ and a potential model of (**g**) $ExbB_6$–$ExbD_4$. **f, g** The models are shown as bottom views (*upper panels*) and oblique views (*lower panels*); for clarity, ExbB TM α-helices are *colored blue* and ExbD TM α-helices *green*

MotA and MotB, respectively, there may be diffusion of ExbB in and out of active complexes (Leake et al. 2006). Studies have also shown that other ExbB–ExbD homologues, the TolQ–TolR complexes, are present in a 4–6:2 stoichiometry (Cascales et al. 2001). Investigations into the organization of their multiple TM α-helices have proposed a model where the TolQ TM α-helices are found on the periphery and the TolR TM α-helices in the interior in the Tol system (Cascales et al. 2001; Zhang et al. 2009). Similar models have been advocated (Braun et al. 2003) for the $MotA_4$–$MotB_2$ complex and (Wille et al. 2013) for the recently identified homologues $SiiB_4$–$SiiA_2$ from *Salmonella* that function in type I secretion system-mediated adhesion and invasion of epithelial cells. In accordance with these homologous models, and by extrapolation from our EM data (Fig. 2e), we propose a possible arrangement of TM α-helices in the $ExbB_4$–$ExbD_2$ (Fig. 3d, f) and the $ExbB_6$–$ExbD_4$ (Fig. 3e, g) complexes. This potential layout resembles the larger oligomer observed by EM and would explain why ExbD tetramers have never been identified. Furthermore, these oligomers would enable rapid formation of active complexes with the cellular surplus of ExbB (Higgs et al. 2002).

Quantitation of Bound Surfactant

Purification of ExbB–ExbD began by solubilizing total membranes in 1 % DDM. Subsequent manipulations used buffers supplemented with 0.02 % DDM. To determine the concentration of detergent in protein-containing samples, 1D NMR spectra were recorded for fractions of SEC-purified complexes. Fractions containing only the running buffer were found to contain 0.018 ± 0.002 % DDM. In combination with parallel protein assays, these experiments revealed two peaks of signal, the first of which is the protein/detergent complex (Fig. 4a). By comparing protein concentrations to detergent concentrations, the protein/detergent complex was estimated to contain 37.1 ± 7.6 % detergent in mass. This value is similar to previous measurements carried out on ExbB–ExbD (35 %) using a

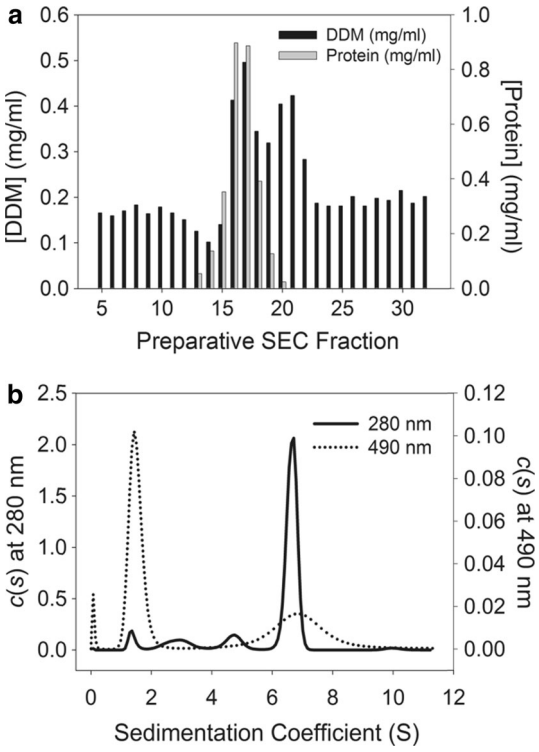

Fig. 4 Quantitation of (**a**) DDM and (**b**) APols associated with ExbB–ExbD. **a** SEC fractions of post-IMAC protein were assayed for protein (absorbance; *gray bars*) and DDM (1D NMR; *black bars*). The first of two peaks of DDM signal is associated with protein elution. The second peak is attributable to free DDM micelles and/or lipids. **b** $c(s)$ analyses of sedimentation velocity data following protein-trapping and supplementation with fluorescent APol identifies a protein/APol complex (6.9 S) and the free APol (1.4–1.5 S). Comparison of protein to each surfactant shows that more APol than DDM binds the $ExbB_4$–$ExbD_2$ complex

different assay (Pramanik et al. 2011). We cannot exclude, however, that some of the quantitated signal (originating from the hydrogen atoms of the terminal methyl group of the detergent's hydrophobic tail) may include some contribution of the acyl chains of endogenous lipids. It is unlikely, however, that those influence very much our estimate of ~82 kDa (~ 160 molecules) of DDM per 139-kDa $ExbB_4$–$ExbD_2$ complex, or an overall mass of ~220 kDa, consistent with BN-PAGE estimates (~240 kDa).

To estimate the amount of APol bound to $ExbB_4$–$ExbD_2$, the complex was trapped with a 5:1 mixture of unlabeled A8-35 and NBD-labeled A8-35 (FAPol) (Zoonens et al. 2007), followed by preparative SEC (120-mL Superdex 200) so as to obtain a monodisperse complex. FAPol, and by extension total APol, was quantitated by its absorption peak at 490 nm (Zoonens et al. 2007) (Fig. S1). Based on assumptions of APol binding (and later revised to the quantitated value), it was empirically determined that using a 3.2–3.5-mass ratio of APol over protein prevents minor aggregation of $ExbB_4$–$ExbD_2$ (Fig. S2). To investigate how much APol is actually bound, this APol-supplemented material was analyzed by SV AUC, with detection at 280 and 490 nm to quantitate the relative protein and APol content, respectively (Ebel 2011). Due to the low absorbance at 490 nm and substantial signals from multiple species, the continuous distribution ($c(s)$) analysis was performed using the 280-nm data, and the resulting model fit parameters used for the 490-nm $c(s)$ analysis (Fig. 4b). The major species at 280 nm (6.9 S) corresponds to the $ExbB_4$–$ExbD_2$ complex together with the APol mixture, the latter's diffuse signal observable at 490 nm. The non-bound APol mixture at 1.4–1.5 S can be seen at 490 nm but absorbs slightly at 280 nm. This sedimentation coefficient is similar to that previously reported for free A8-35 particles (Gohon et al. 2006). After correcting for FAPol absorbance at 280 nm, we calculated that the preparation contains ~3.2 g of total APol per g of total protein, confirming the empirical supplementation of SEC-purified protein/APol complex. At the 6.9 S peak, complex-associated APol represents 1.2–1.5 g per g of protein. Some uncertainty arises from the low signal at 490 nm and applying the 280-nm fit parameters to the 490-nm data. Attempts at fitting the 490-nm data independently led to inconsistent results of peak integration. The apparent R_S calculated for the free APol particles (2.2 nm) is smaller than the 3.15 nm previously reported (Gohon et al. 2006), reflecting difficulties in obtaining a unique solution for the frictional ratio, possibly due to the presence of endogenous lipids. For this reason, sedimentation data were only used to estimate the mass ratio of APol/protein, which is similar to that found in other studies (Zoonens et al. 2007). A ratio of 1.2–1.5 g APol per g protein corresponds to 167–208 kDa, resulting in a calculated mass of 305–347 kDa for the $ExbB_4$–$ExbD_2$/APol complex. This amount of bound APols is on the high side for a complex with 14 predicted TM α-helices, compared to bacteriorhodopsin (7 α-helices), which binds ~54 kDa of A8-35 (Gohon et al. 2008). Whereas bacteriorhodopsin is a helical bundle, the proposed TM α-helix arrangement of ExbB–ExbD (Fig. 3d) would be more convoluted, as seen for the TRPV1 complex (Liao et al. 2014), and therefore, bind more APols. These values are consistent with BN-PAGE mass estimates (Fig. 1b, lane 5), taking into account that Coomassie-bound MPs tend to migrate further than their soluble protein counterparts (Heuberger et al. 2002; Wittig et al. 2010) and that the presence of the negatively charged A8-35 may accelerate the migration.

Small-Angle Scattering of Protein/APol Complexes

SAXS and SANS provided independent information about the dimensions and shape of the $ExbB_4$–$ExbD_2$ complex

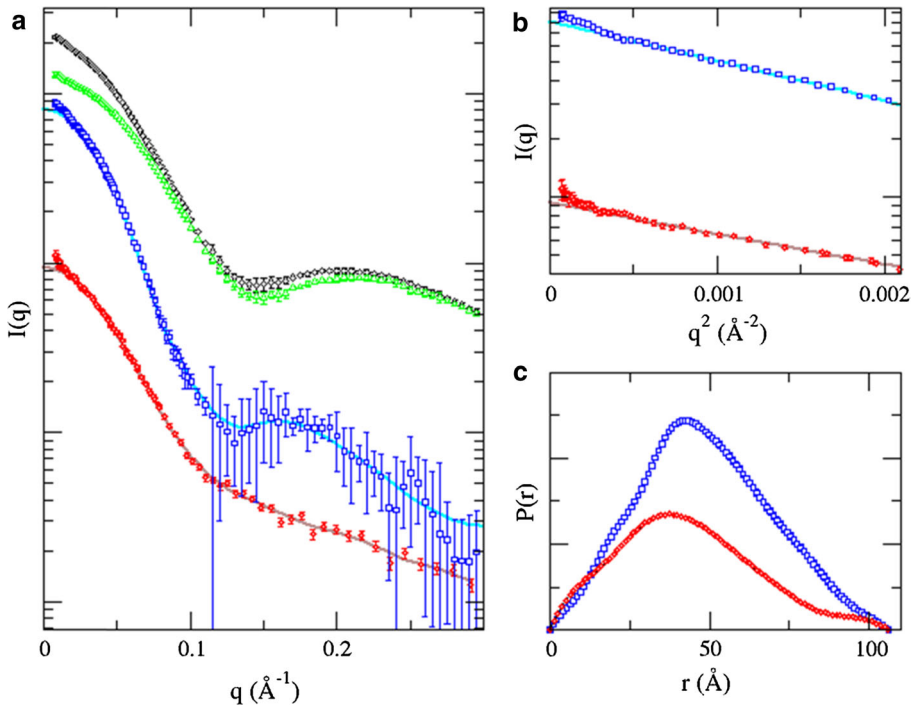

Fig. 5 Analysis by SAXS and SANS of the ExbB–ExbD/APol complex. **a** SAXS (*black diamonds*) and SANS (*red circles*) scattering data collected from APol-trapped protein. The SAXS contribution from free APol particles (*green triangles*) was subtracted to give the scattering intensity that corresponds to the APol-trapped protein complex alone (*blue squares*). The SAXS data are not normalized to absolute scale. **b** Guinier fit to the SAXS (*blue squares*) and SANS (*red circles*) data shown in (**a**). The resultant R_g values are 37.3 Å for the SAXS data (protein + bound APol) and 33.8 Å for the SANS data (protein alone). **c** The $P(r)$ functions derived from the data in (**a**). The *solid lines* shown in (**a**) represent the inverse transform of the $P(r)$ functions. The two $P(r)$ functions are scaled for clarity. The D_{max} values are 106 Å for both

and the relative arrangement of its protein and surfactant components. After trapping in hydrogenated APol, protein/APol complexes were purified on a 120-mL Superdex 200 SEC column. Pooled fractions containing monodisperse complexes were concentrated in 150-kDa MWCO concentrators and supplemented with deuterated A8-35 (DAPol; Gohon et al. 2004, 2006). The resulting mixture contained a total APol (APol + DAPol) mass ratio of 11.4:1, with the deuterated component in excess by 8.5-fold (calculated using 1.2 g of bound APol per g protein). This large excess was chosen to ensure that the DAPol is the dominant APol, thus providing for contrast matching at a high percentage of D_2O (the contrast-matching point of APol is ~23.5 % D_2O, that of DAPol ~85 %; Gohon et al. 2004). Unexpectedly, the addition of excess APol resulted in the appearance of minor amounts of smaller complexes, as detected by analytical SEC and AUC (data not shown). These complexes of ~3.5 and 5 nm R_S first appeared after ~1 week and tended to increase in proportion as a function of total APol concentration in samples. This suggests that interactions between the protein components of the complex are labile, so that complexes with lower stoichiometries of ExbB–ExbD are produced upon exposure to an excess of APol, potentially due to collisions between free APol molecules with protein/APol complexes (Zoonens et al. 2007). The smaller complexes, however, were present in minor amounts and were estimated to have little influence on SAXS and SANS measurements.

SAXS measurements of diluted APol and DAPol solutions showed similar scattering profiles (Fig. S3) with R_g of ~2.4 nm, agreeing with values found by SANS (Gohon et al. 2006). The diluted APol-supplemented protein/APol scattering profile is shown in Fig. 5a. The scattering contribution from free APol particles, determined by scaling the free APol scattering intensity by a factor of 2.5, was then subtracted from total scattering by the protein/APol sample. The amount of matched free APol was compared to the supplemented protein/APol complex (leaving only bound APol), resulting in a APol/protein mass ratio of 1.3, consistent with our AUC results. Owing to contrast matching, the SANS intensity does not contain contributions from either the free or the bound APol (Fig. 5a). The two sets of small-angle scattering data were compared in terms of R_g (Fig. 5b) and $P(r)$ (Fig. 5c). As expected, the SAXS data of the protein/APol complex resulted in a larger

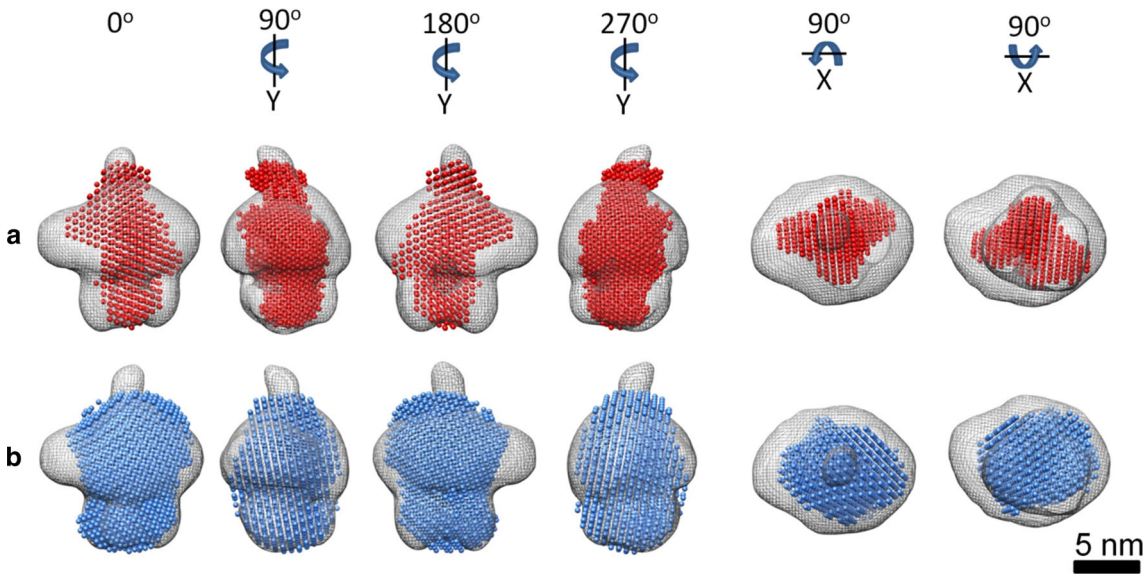

Fig. 6 Shape modeling results of small-angle scattering data and comparison with EM observations. After averaging multiple DAMMIN reconstructions and selecting only high-occupancy positions, we compare the SANS-derived (**a**) and SAXS-derived (**b**) bead models to a composite map of EM structural states. These models are consistent with each other: they have similar size along the *y*-axis and the overall dimensions of these models are compatible with the EM composite map. The SAXS model occupies a larger volume due to the contribution of APol. The SANS model contains less volume in the TM region due to contrast matching the APol

R_g (37.3 Å) than that of the contrast-matched SANS data (33.8 Å). However, both measurements showed similar D_{max} values (106 Å), suggesting that the decrease in R_g was localized to the shorter axis of our $ExbB_4$–$ExbD_2$ EM models, identified as the TM region (Fig. 2c; red bracket).

Shape modeling of the SAXS and SANS data was performed using DAMMIN (Svergun 1999). For the SANS data shape modeling, 20 individual models were generated and averaged together following standard procedures (Volkov and Svergun 2003), resulting in the total spread region (TSR). As the TSR represents the sum of all computational outcomes, they were reduced to the bead positions most frequently occupied by the models (most populated volume). The cut-off volume for this reduction was chosen to match the molecular weight based on scattering (see Eq. 1 in Materials and Methods). The contrast-matched SANS data, contributed only by the protein, yielded a molecular mass of 127 ± 13 kDa, consistent with expectations. This value was used to establish the cut-off volume of 1.56×10^5 Å^3 of the average SANS model. The SAXS data shape modeling followed a similar protocol, but, due to the non-uniform electron density in the complex, neither the molecular weight nor a cut-off volume could be determined. For consistency, the same fraction of the TSR was used as for the SANS data. Fig. 6 compares the SANS-derived (Fig. 6a) and the SAXS-derived (Fig. 6b) bead models to a composite EM map (shown as a gray mesh). This map combines the three structural states that the $ExbB_4$–$ExbD_2$ complex adopts in detergent (not weight-averaged). Since APols allow this conformational flexibility (Fig. 2d), it is expected that the scattering data lead to a weight-averaged mixture of the dynamic states. Given that the SAXS-derived DAMMIN model is not expected to correctly represent the electron density difference between protein and APol, Fig. 6b can only confirm the general dimensions of the EM composite model. In contrast, Fig. 6a shows the model of protein-only contributions from scattering data; there is substantially less volume in the TM region compared to Fig. 6b (where the extra volume is APol) and to the EM composite map (where the extra volume is detergent). Also, reducing the TSR cut-off volume (data not shown) reveals a hole below the TM region that resembles the structural state where the ExbB cytoplasmic domains form a dimer of dimers. Furthermore, the SANS model contains two extensions (extended and membrane-parallel) of volume occupying approximately the same positions as the ExbD C-terminus dimer in the EM maps. Considering that these DAMMIN models represent a cut-off occupancy average of multiple possible reconstructions and that the final shape is usually slightly distorted for globular particles with small cavities (Volkov and Svergun 2003), small-angle scattering by $ExbB_4$–$ExbD_2$/APol complexes appears largely consistent with EM observations and will be valuable in future studies of the ExbB–ExbD–TonB complexes.

Conclusion

Studies of MPs usually begin by thorough screening of various detergents. Each membrane protein will have its own ideal surfactant for the anticipated studies; which surfactant will be best tolerated varies from one protein to the next. As a complement to studies of ExbB–ExbD in our optimal detergent, we investigated similarities and differences of the MP complex in APols. In the case study presented here, we document the contribution of APols to increased thermal stability, report that they permit crucial conformational changes thought to be linked to in vivo function, and explore their use for small-angle studies of $ExbB_4$–$ExbD_2$ complexes with the protein stabilized and the surfactant contrast matched.

Acknowledgments Particular thanks are due to F. Giusti (UMR 7099, Paris) for synthesizing the deuterated and the fluorescent amphipols used in this project. This work was supported by an operating grant to J.W.C. from the Canadian Institutes of Health Research (CIHR reference number 200709MOP-178048-BMA-CFAA-11449). The Groupe d'étude des protéines membranaires (GÉPROM), supported by the Fonds de la recherche en santé du Québec (FRSQ), awarded a *Projet Novateur* to J.W.C. A.S. was awarded fellowships from the CREATE program, *Cellular Dynamics of Macromolecular Complexes*, Natural Sciences and Engineering Research Council (NSERC) of Canada; from GÉPROM; and from the F.C. Harrison and the Rozanis Funds, Department of Microbiology and Immunology, McGill University. Work in UMR 7099 was supported by the French Centre National de la Recherche Scientifique (CNRS), by Université Paris-7 Denis Diderot, and by grant "DYNAMO", ANR-11-LABX-0011-01, from the French "Initiative d'Excellence" program. Canada Foundation for Innovation provided infrastructure for the Facility for Electron Microscope Research, McGill University; www.medicine.mcgill.ca/femr/home.html. We appreciate support from Isabelle Rouiller for EM studies. Tara Sprules, manager of the Quebec/Eastern Canada High Field NMR Facility,www.nmrlab.mcgill.ca, guided NMR experiments to quantitate detergent. Research at the Bio-SANS (Center for Structural Molecular Biology) was supported by the U.S. Department of Energy's Office of Biological and Environmental Research. Research at Oak Ridge National Laboratory's High Flux Isotope Reactor was sponsored by the Scientific User Facilities Division, Office of Basic Energy Sciences, U.S. Department of Energy. Oak Ridge National Laboratory is managed by UT-Battelle, LLC for the U.S. Department of Energy. Use of the National Synchrotron Light Source, Brookhaven National Laboratory, was supported by the U.S. Department of Energy, Office of Science, Office of Basic Energy Sciences, under Contract No. DE-AC02-98CH10886. We appreciate the access to AF4 equipment in the laboratory of Françoise Winnik at the Université de Montréal. This work was facilitated by computing resources from CLUMEQ, under Compute/Calcul Canada. We appreciate laboratory support from Nathalie Croteau and suggestions on the manuscript by J. A. Kashul.

References

Aitken A, Learmonth MP (2002) Protein determination by UV absorption. In: Walker JM (ed) The protein protocols handbook, 2nd edn. Humana Press, Clifton, pp 3–6

Alexandrov AI, Mileni M, Chien EYT, Hanson MA, Stevens RC (2008) Microscale fluorescent thermal stability assay for membrane proteins. Structure 16:351–359

Allaire M, Yang L (2011) Biomolecular solution X-ray scattering at the National Synchrotron Light Source. J Synchrotron Radiat 18:41–44

Arunmanee W, Harris JR, Lakey JH (2014) Outer membrane protein F stabilised with minimal amphipol forms linear arrays and LPS-dependent 2D crystals. J Membr Biol. doi:10.1007/s00232-014-9640-5

Baker KR, Postle K (2013) Mutations in *Escherichia coli* ExbB transmembrane domains identify scaffolding and signal transduction functions and exclude participation in a proton pathway. J Bacteriol 195:2898–2911

Braun V, Gaisser S, Herrmann C, Kampfenkel K, Killmann H, Traub I (1996) Energy-coupled transport across the outer membrane of *Escherichia coli*: ExbB binds ExbD and TonB in vitro, and leucine 132 in the periplasmic region and aspartate 25 in the transmembrane region are important for ExbD activity. J Bacteriol 178:2836–2845

Braun TF, Al-Mawsawi LQ, Kojima S, Blair DF (2003) Arrangement of core membrane segments in the MotA/MotB proton-channel complex of *Escherichia coli*. Biochemistry 43:35–45

Cascales E, Lloubès R, Sturgis JN (2001) The TolQ–TolR proteins energize TolA and share homologies with the flagellar motor proteins MotA–MotB. Mol Microbiol 42:795–807

Charvolin D, Picard M, Huang L-S, Berry EA, Popot J-L (2014) Solution behavior and crystallization of cytochrome bc_1 in the presence of amphipols. J Membr Biol (submitted)

Chen JZ, Grigorieff N (2007) SIGNATURE: a single-particle selection system for molecular electron microscopy. J Struct Biol 157:168–173

Chu BH, Peacock RS, Vogel H (2007) Bioinformatic analysis of the TonB protein family. Biometals 20:467–483

Cölfen H, Antonietti M (2000) Field-flow fractionation techniques for polymer and colloid analysis. In: Schmidt M (ed) New developments in polymer analytics I. Springer, Berlin, pp 67–187

Dahmane T, Damian M, Mary S, Popot J-L, Banères J-L (2009) Amphipol-assisted in vitro folding of G protein-coupled receptors. Biochemistry 48:6516–6521

Ebel C (2011) Sedimentation velocity to characterize surfactants and solubilized membrane proteins. Methods 54:56–66

Giddings J (1993) Field-flow fractionation: analysis of macromolecular, colloidal, and particulate materials. Science 260:1456–1465

Giusti F, Popot J-L, Tribet C (2012) Well-defined critical association concentration and rapid adsorption at the air/water interface of a short amphiphilic polymer, amphipol A8-35: a study by Förster resonance energy transfer and dynamic surface tension measurements. Langmuir 28:10372–10380

Giusti F, Rieger J, Catoire L, Qian S, Calabrese AN, Watkinson TG, Casiraghi M, Radford SE, Ashcroft AE, Popot J-L (2014) Synthesis, characterization and applications of a perdeuterated amphipol. J Membr Biol. doi:10.1007/s00232-014-9656-x

Gohon Y, Pavlov G, Timmins P, Tribet C, Popot J-L, Ebel C (2004) Partial specific volume and solvent interactions of amphipol A8-35. Anal Biochem 334:318–334

Gohon Y, Giusti F, Prata C, Charvolin D, Timmins P, Ebel C, Tribet C, Popot J-L (2006) Well-defined nanoparticles formed by hydrophobic assembly of a short and polydisperse random terpolymer, amphipol A8-35. Langmuir 22:1281–1290

Gohon Y, Dahmane T, Ruigrok RW, Schuck P, Charvolin D, Rappaport F, Timmins P, Engelman DM, Tribet C, Popot J-L, Ebel C (2008) Bacteriorhodopsin/amphipol complexes: structural and functional properties. Biophys J 94:3523–3537

Harpaz Y, Gerstein M, Chothia C (1994) Volume changes on protein folding. Structure 2:641–649

Hayashi Y, Matsui H, Takagi T, Takagi T (1989) Membrane protein molecular weight determined by low-angle laser light-scattering photometry coupled with high-performance gel chromatography. In: Sidney Fleischer BF (ed) Methods enzymol. Academic Press, Boston, pp 514–528

Heller WT (2010) Small-angle neutron scattering and contrast variation: a powerful combination for studying biological structures. Acta Crystallogr D Biol Crystallogr 66:1213–1217

Heuberger EHML, Veenhoff LM, Duurkens RH, Friesen RHE, Poolman B (2002) Oligomeric state of membrane transport proteins analyzed with blue native electrophoresis and analytical ultracentrifugation. J Mol Biol 317:591–600

Higgs PI, Larsen RA, Postle K (2002) Quantification of known components of the *Escherichia coli* TonB energy transduction system: TonB, ExbB, ExbD and FepA. Mol Microbiol 44:271–281

Holloway PW (1973) A simple procedure for removal of triton X 100 from protein samples. Anal Biochem 53:304–308

Jana B, Manning M, Postle K (2011) Mutations in the ExbB cytoplasmic carboxy terminus prevent energy-dependent interaction between the TonB and ExbD periplasmic domains. J Bacteriol 193:5649–5657

Kampfenkel K, Braun V (1992) Membrane topology of the *Escherichia coli* ExbD protein. J Bacteriol 174:5485–5487

Kampfenkel K, Braun V (1993) Topology of the ExbB protein in the cytoplasmic membrane of *Escherichia coli*. J Biol Chem 268:6050–6057

Krewulak KD, Vogel HJ (2011) TonB or not TonB: is that the question? Biochem Cell Biol 89:87–97

Leake MC, Chandler JH, Wadhams GH, Bai F, Berry RM, Armitage JP (2006) Stoichiometry and turnover in single, functioning membrane protein complexes. Nature 443:355–358

Liao M, Erhu C, Julius D, Cheng T (2014) Structure of the TRPV1 ion channel determined by electron cryo-microscopy. Nature 504:107–112

Lynn GW, Heller W, Urban V, Wignall GD, Weiss K, Myles DAA (2006) Bio-SANS—A dedicated facility for neutron structural biology at Oak Ridge National Laboratory. Phys B Condens Matter 385–386(Part 2):880–882

Maslennikov I, Kefala G, Johnson C, Riek R, Choe S, Kwiatkowski W (2007) NMR spectroscopic and analytical ultracentrifuge analysis of membrane protein detergent complexes. BMC Struct Biol 7:74

Nikaido H (2003) Molecular basis of bacterial outer membrane permeability revisited. Microbiol Mol Biol Rev 67:593–656

Ohi M, Li Y, Cheng Y, Walz T (2004) Negative staining and image classification—powerful tools in modern electron microscopy. Biol Proced Online 6:23–34

Ollis AA, Postle K (2011) The same periplasmic ExbD residues mediate in vivo interactions between ExbD homodimers and ExbD–TonB heterodimers. J Bacteriol 193:6852–6863

Ollis AA, Kumar A, Postle K (2012) The ExbD periplasmic domain contains distinct functional regions for two stages in TonB energization. J Bacteriol 194:3069–3077

Pace CN, Vajdos F, Fee L, Grimsley G, Gray T (1995) How to measure and predict the molar absorption coefficient of a protein. Protein Sci 4:2411–2423

Pawelek PD, Croteau N, Ng-Thow-Hing C, Khursigara CM, Moiseeva N, Allaire M, Coulton JW (2006) Structure of TonB in complex with FhuA, E. coli outer membrane receptor. Science 312:1399–1402

Perlmutter JD, Popot J-L, Sachs JN (2014) Molecular dynamics simulations of a membrane protein/amphipol complex. J Membr Biol. doi:10.1007/s00232-014-9690-8

Popot J-L, Althoff T, Bagnard D, Banères J-L, Bazzacco P, Billon-Denis E, Catoire LJ, Champeil P, Charvolin D, Cocco MJ, Crémel G, Dahmane T, de la Maza LM, Ebel C, Gabel F, Giusti F, Gohon Y, Goormaghtigh E, Guittet E, Kleindschmidt JH, Kuhlbrandt W, Le Bon C, Martinez KL, Picard M, Pucci B, Sachs JN, Tribet C, van Heijenoort C, Wien F, Zito F, Zoonens M (2011) Amphipols from A to Z. Annu Rev Biophys 40:379–408

Pramanik A, Zhang F, Schwarz H, Schreiber F, Braun V (2010) ExbB protein in the cytoplasmic membrane of *Escherichia coli* forms a stable oligomer. Biochemistry 49:8721–8728

Pramanik A, Hauf W, Hoffmann J, Cernescu M, Brutschy B, Braun V (2011) Oligomeric structure of ExbB and ExbB-ExbD isolated from *Escherichia coli* as revealed by LILBID mass spectrometry. Biochemistry 50:8950–8956

Roy A, Nury H, Wiseman B, Sarwan J, Jault J-M, Ebel C (2013) Sedimentation velocity analytical ultracentrifugation in hydrogenated and deuterated solvents for the characterization of membrane proteins. In: Rapaport D, Herrmann JM (eds) Membrane biogenesis. Humana Press, New York, pp 219–251

Salvay A, Ebel C (2006) Analytical ultracentrifuge for the characterization of detergent in solution. In: Wandrey C, Cölfen H (eds) Analytical ultracentrifugation VIII. Springer, Berlin, pp 74–82

Scheres SHW, Núñez-Ramírez R, Sorzano COS, Carazo JM, Marabini R (2008) Image processing for electron microscopy single-particle analysis using XMIPP. Nat Protoc 3:977–990

Schneider CA (2012) NIH Image to ImageJ: 25 years of image analysis. Nat Meth 9:671–675

Schuck P (2000) Size-distribution analysis of macromolecules by sedimentation velocity ultracentrifugation and Lamm equation modeling. Biophys J 78:1606–1619

Svergun DI (1992) Determination of the regularization parameter in indirect-transform methods using perceptual criteria. J Appl Crystallogr 25:495–503

Svergun DI (1999) Restoring low resolution structure of biological macromolecules from solution scattering using simulated annealing. Biophys J 76:2879–2886

Sverzhinsky A, Fabre L, Cottreau AL, Biot-Pelletier DMP, Khalil S, Bostina M, Rouiller I, Coulton JW (2014) Coordinated rearrangements between cytoplasmic and periplasmic domains of the membrane protein complex ExbB–ExbD of *Escherichia coli*. Structure 22:791–797

Tribet C, Audebert R, Popot J-L (1996) Amphipols: polymers that keep membrane proteins soluble in aqueous solutions. Proc Natl Acad Sci USA 93:15047–15050

Volkov VV, Svergun DI (2003) Uniqueness of ab initio shape determination in small-angle scattering. J Appl Crystallogr 36:860–864

Wagner M, Pietsch C, Tauhardt L, Schallon A, Schubert US (2014) Characterization of cationic polymers by asymmetric flow field-flow fractionation and multi-angle light scattering—a comparison with traditional techniques. J Chromatogr A 1325:195–203

Wasiak S, Legendre-Guillemin V, Puertollano R, Blondeau F, Girard M, de Heuvel E, Boismenu D, Bell AW, Bonifacino JS, McPherson PS (2002) Enthoprotin: a novel clathrin-associated protein identified through subcellular proteomics. J Cell Biol 158:855–862

Wille T, Wagner C, Mittelstädt W, Blank K, Sommer E, Malengo G, Döhler D, Lange A, Sourjik V, Hensel M, Gerlach RG (2013) SiiA and SiiB are novel type I secretion system subunits controlling SPI4-mediated adhesion of *Salmonella enterica*. Cell Microbiol 16(2):161–178

Wittig I, Beckhaus T, Wumaier Z, Karas M, Schägger H (2010) Mass estimation of native proteins by blue native electrophoresis: Principles and practical hints. Mol Cell Proteomics 9:2149–2161

Yang L (2013) Using an in-vacuum CCD detector for simultaneous small- and wide-angle scattering at beamline X9. J Synchrotron Radiat 20:211–218

Yang Z, Fang J, Chittuluru J, Asturias FJ, Penczek PA (2012) Iterative stable alignment and clustering of 2D transmission electron microscope images. Structure 20:237–247

Zhang XY-Z, Goemaere EL, Thomé R, Gavioli M, Cascales E, Lloubès R (2009) Mapping the interactions between *Escherichia coli* Tol subunits: Rotation of the TolR transmembrane helix. J Biol Chem 284:4275–4282

Zoonens M, Popot J-L (2014) Amphipols for each season. J Membr Biol. doi:10.1007/s00232-014-9666-8

Zoonens M, Giusti F, Zito F, Popot J-L (2007) Dynamics of membrane protein/amphipol association studied by Förster resonance energy transfer: implications for in vitro studies of amphipol-stabilized membrane proteins. Biochemistry 46: 10392–10404

Zoonens M, Zito F, Martinez KL, Popot J-L (2014) Amphipols: a general introduction and some protocols. In: Mus-Veteau I (ed) Membrane protein production for structural analysis. Springer, New York